# Tropical Western Pacific: A Year in Darwin

*C. N. Long, J. H. Mather, and S. A. McFarlane*
*Pacific Northwest National Laboratory*
*Richland, Washington*

*L. Jones, W. M. Porch, and A. Haruta*
*Los Alamos National Laboratory*
*Los Alamos, New Mexico*

## Introduction

In March 2002, the third Tropical Western Pacific (TWP) Atmospheric Radiation Measurement (ARM) site was installed adjacent to the international airport in Darwin, Australia (12.42 S latitude, 130.89 E longitude; Figure 1). Darwin is located on the northwest coast of Australia, adjacent to the


**Figure 1**. A map of the Tropical Western Pacific/Maritime continent region showing the locations of the three TWP ARM sites.

Timor Sea and the Maritime Continent region. Darwin experiences a strong annual monsoon cycle. The "dry" season corresponds to the austral winter months (June-August) while the "wet" season occurs during the austral summer (December-February).

Figure 2 presents a map of the Darwin region. As seen from this figure, Darwin is nearly surrounded by water. The layout of the Darwin ARM site and a photograph showing the instrument field as well as the containers housing instruments and computers is shown in Figures 3 and 4. The Darwin site is located on the grounds of the local office of the Bureau of Meteorology. Staff at the meteorology office assist ARM technicians in the maintenance of the Darwin site.

The Darwin site has now been operating for approximately one year. The remainder of this paper will look at the first year of data obtained at the Darwin site. A particular emphasis has been placed on examining the nature of the annual cycle which is much more pronounced than at the TWP sites at Manus and Nauru.


**Figure 2**. Map of the Darwin area.

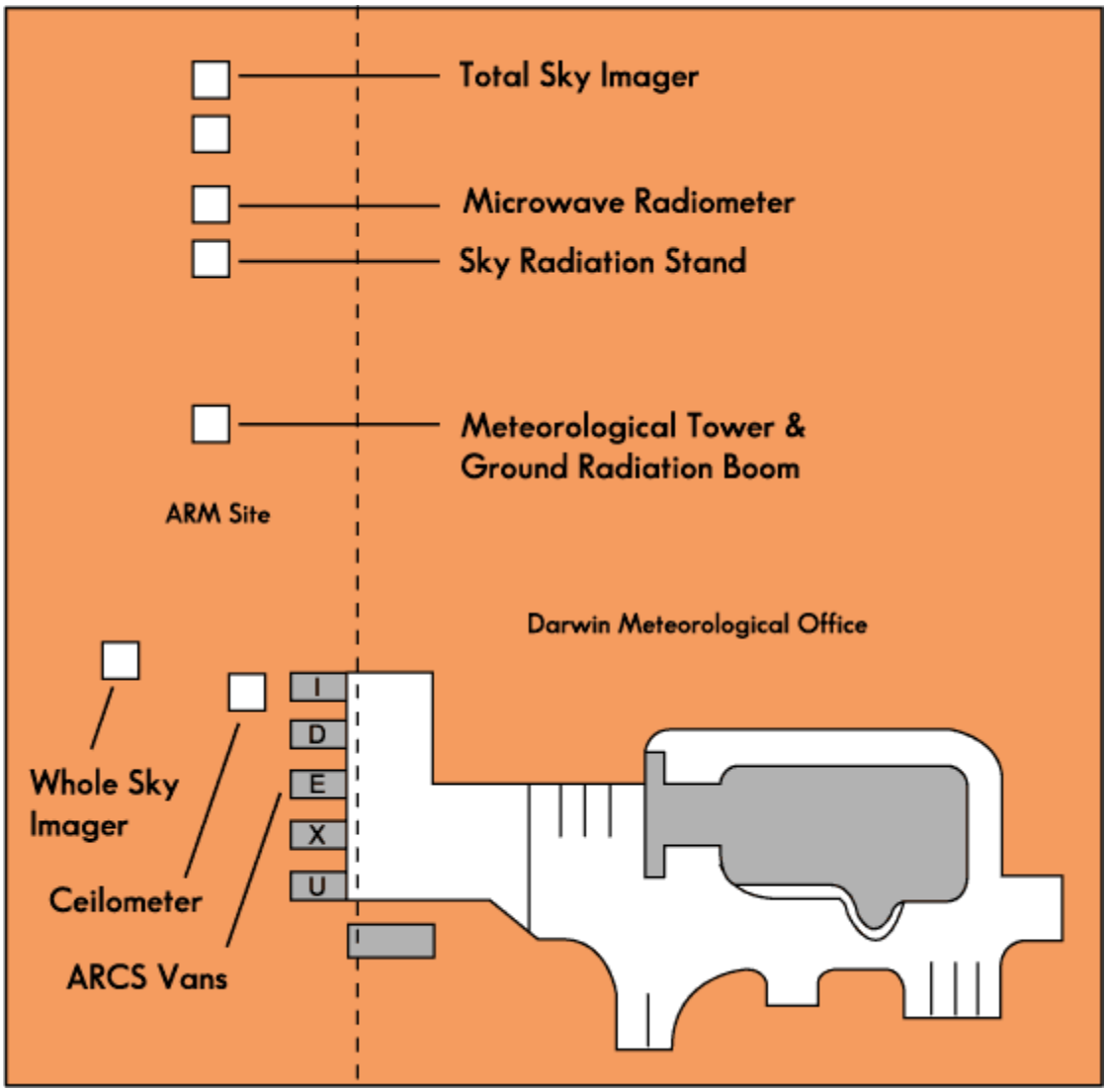


**Figure 3**. Layout of the Darwin site.

## Meteorological and Radiation Observations

Nearly all meteorological variables illustrate the Darwin annual cycle. Figure 5 shows a few measurements from the surface meteorological suite. Though there is not a large temperature swing, there is a distinct minimum during winter. Surface pressure is seen to peak during the dry season while the pressure is low during the wet season when this is a region of large-scale surface convergence. The time series in daily precipitation clearly shows that most of the year's rainfall occurs during the summer months.

The time series of water vapor column from the microwave radiometer in Figure 6 also shows a distinct annual cycle. Low column water amounts prevail during the winter while higher amounts are found during winter although there are large departures toward higher column amounts that occur during the

**Figure 4**. View of the instrument field.

dry season. In Figure 7 the column water vapor data have been re-plotted as frequency distributions. In this figure the data have been segregated by season.

In Figure 8, vertical distributions of cloud base probability reported by the ceilometer are shown. These data were segregated according to the same seasonal divisions that were used to produce the microwave radiometer distributions in Figure 7. These data show that convective clouds (which tend to have a low cloud base) are much more likely during the spring/summer season than fall/winter.

The annual cycle in moisture and cloudiness has a significant impact on the surface radiation budget. This relationship is illustrated in Figure 9. This graph displays three quantities related to cloudiness and its impact on solar radiation: the monthly averages of sky cover, percent of the daylight period that was detected as completely clear-sky, and the ratio of the measured over clear-sky downwelling shortwave (SW) irradiance. The "dry" months (June, July, and August) show the greatest occurrence of completely clear skies, low average sky cover amounts, and the largest measured/clear SW ratio values. In

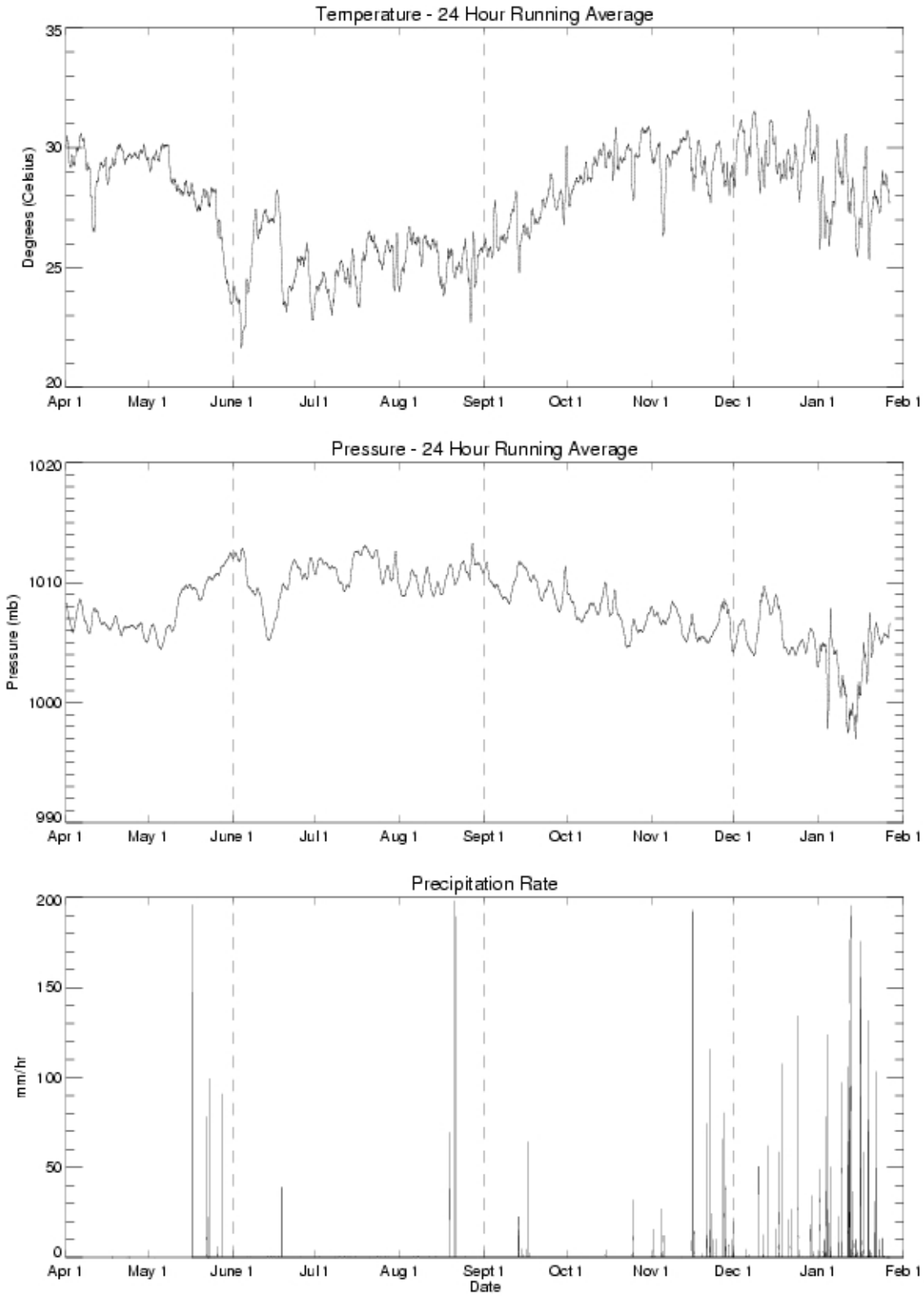


**Figure 5**. Time series of temperature, pressure, and precipitation.

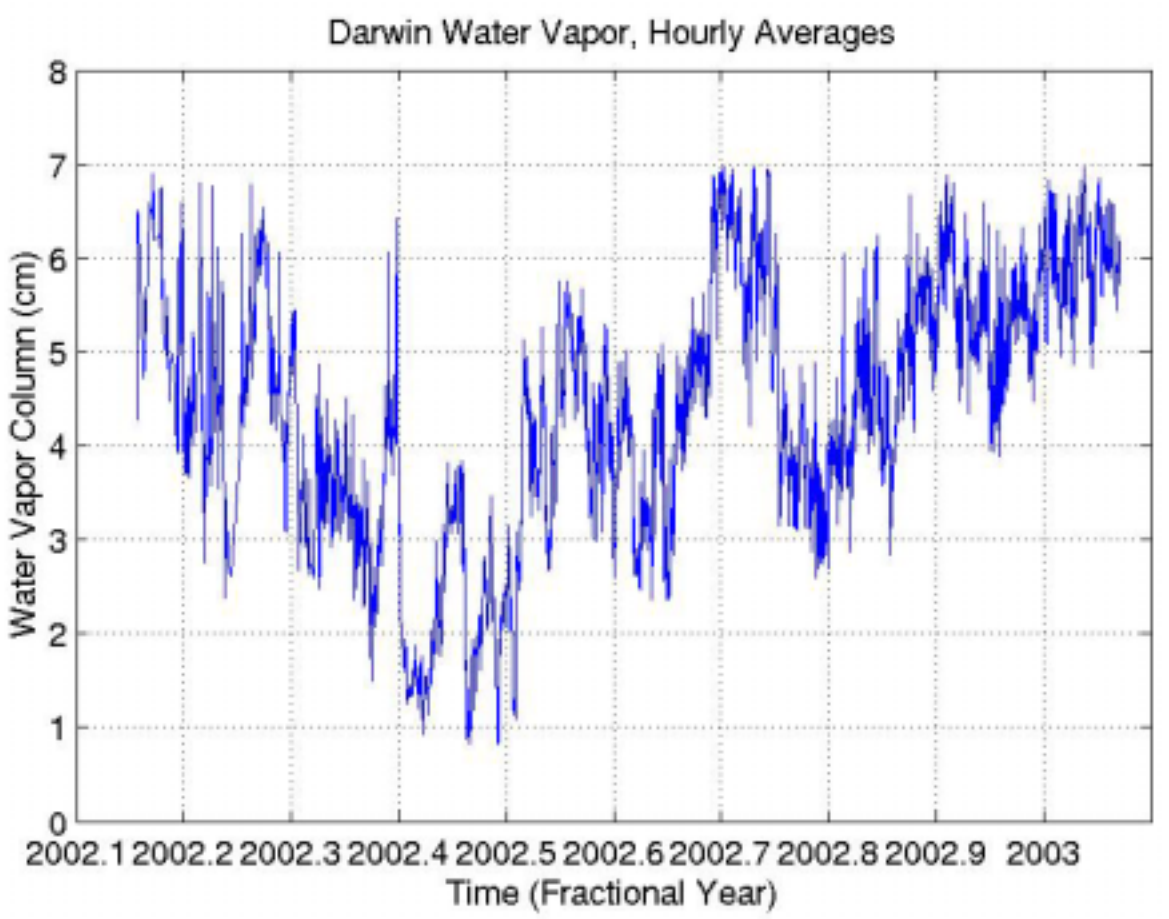


**Figure 6**. Time series of hourly averaged water vapor from the microwave radiometer. Extreme values associated with precipitation events have been removed.

contrast, the plot shows that completely clear skies are rare during the "wet" season (December, January, and February). The wet season exhibits high average sky cover amounts, which results in lower measured/clear SW ratio values because the clouds tend to decrease the amount of downwelling SW reaching the surface.

The SW ratio depicted in Figure 9 is driven primarily by clouds. The net radiative flux into the surface, which is the quantity responsible for surface heating, is also affected by clouds but other factors affect this quantity as well. Figure 10 shows the annual cycle of the net radiative flux as well as its longwave (LW) and SW components. The net flux is defined as the net flux into the ground or the downwelling flux minus the upwelling flux. As one might expect, the net SW was lowest during the wet season. However, the net SW was also low in May, June, and July even though these are dry months with the greatest measured/clear SW ratios and most frequent occurrence of clear skies. (Figure 9). This latter period corresponds with the southern hemisphere winter, when the solar declination angle reaches its northern-most position, and thus the incoming top of the atmosphere SW irradiance reaches its minimum in the southern hemisphere. The low sun angles partially compensate for the effect of the clear skies and reduced sky cover amounts.

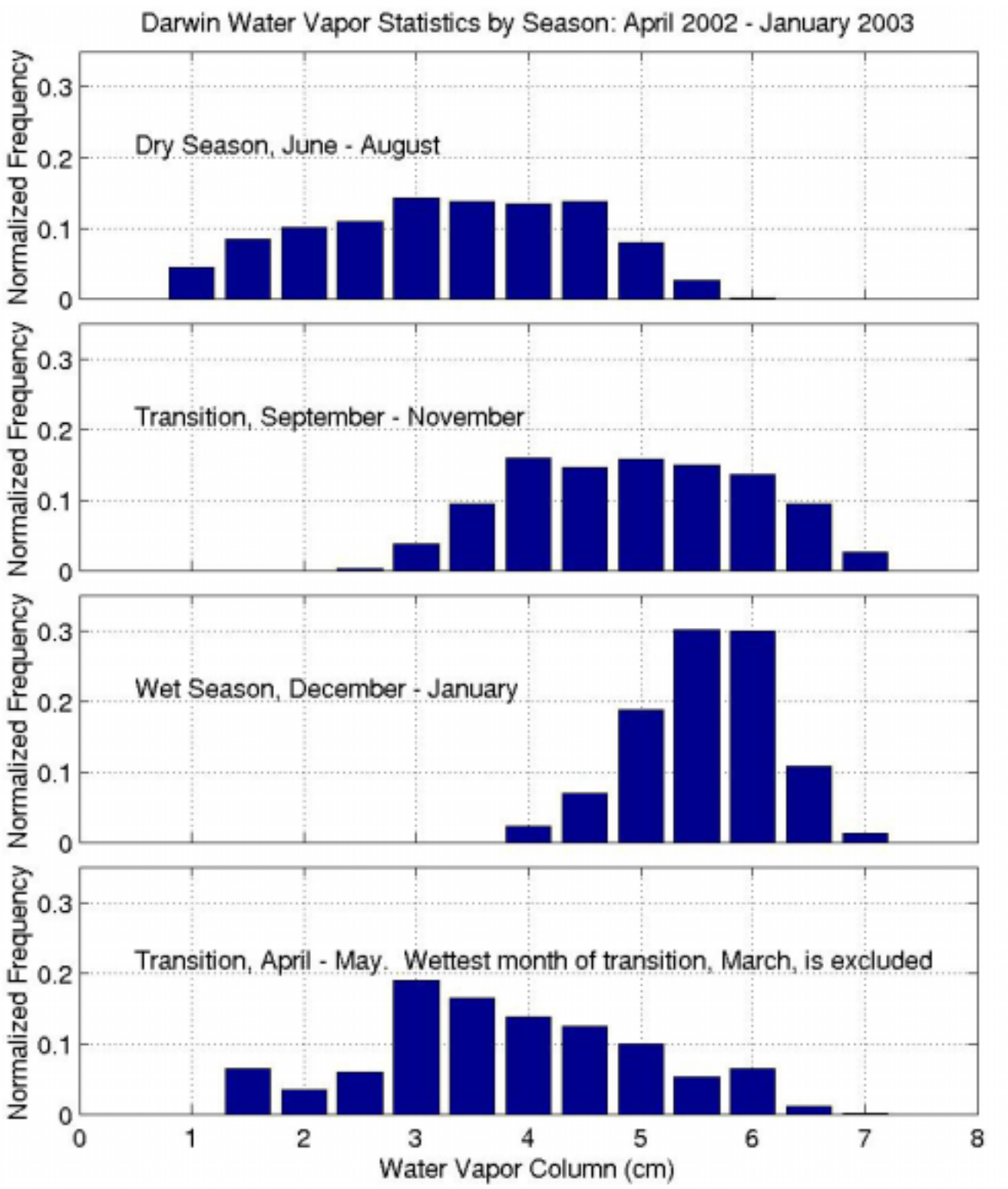


**Figure 7**. Frequency distributions of microwave radiometer column water vapor as a function of season. The time periods were chosen to roughly correspond (from the top down) winter dry season, spring transition (pre-monsoon), wet season, autumn transition (post-monsoon).

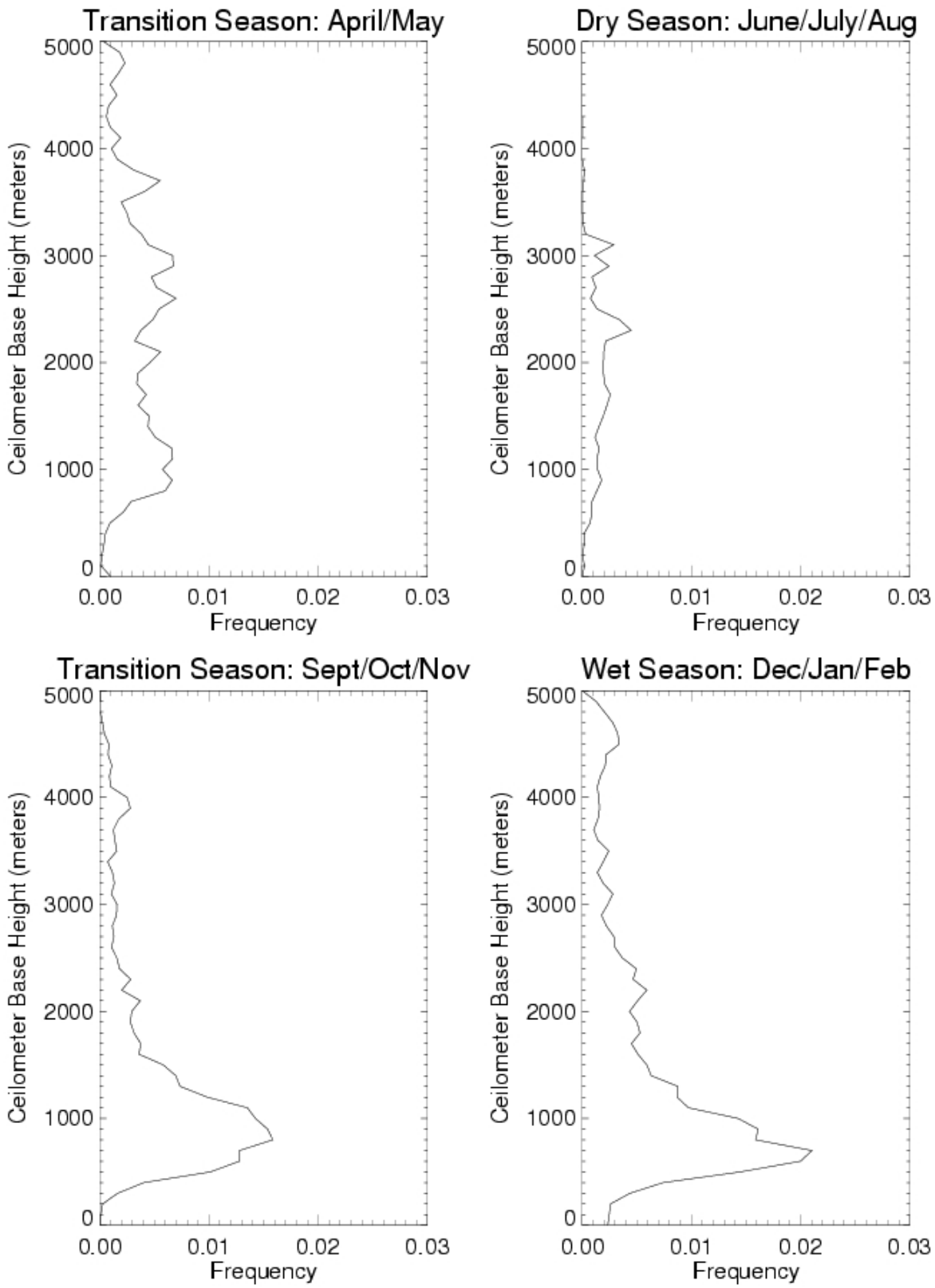


**Figure 8**. Cloud base height distributions obtained from the Vaisala ceilometer.

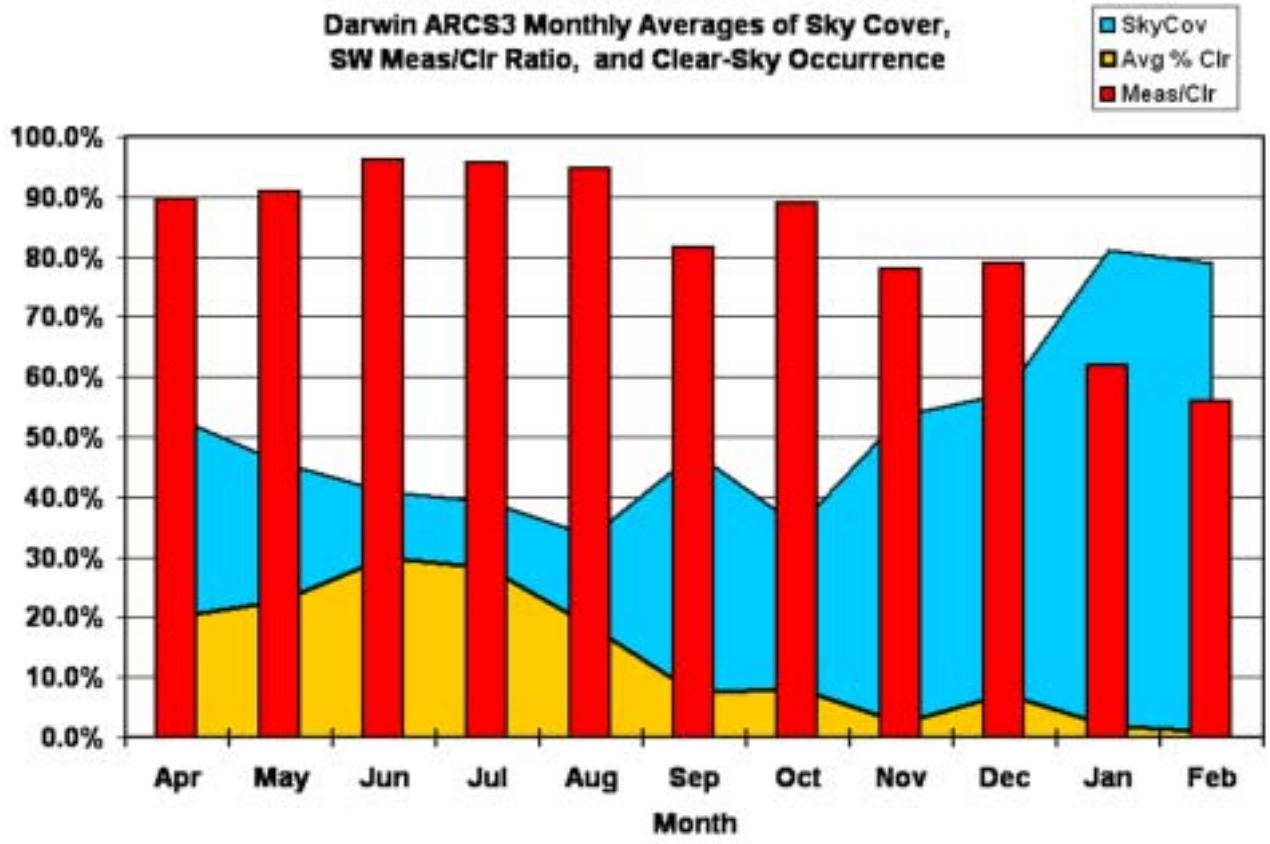


**Figure 9**. Monthly averages of sky cover (blue), percent of daylight period detected as clear-sky (yellow), and the ratio of the measured over clear-sky downwelling SW irradiance (red).

Turning to the LW, the dry season features the minimum downwelling LW irradiances due to the clear skies (Figures 8 and 9) and low column water vapor amounts (Figures 6 and 7). At the same time, the ground surface itself stays warm due to the moderate climate (actually the warmest soil temperatures occur during the winter), and emits significant upwelling LW radiation all year round. Thus, the net LW is the most negative during the dry periods, which, in conjunction with the smaller net SW, results in Darwin's smallest net surface radiative energy budget occurring during the dry season. Conversely, the increase in downwelling LW due to more moist atmospheric conditions (Figures 6 and 7) and proliferation of low cloud bases (Figure 8) produce the least negative net LW, and in conjunction with the net SW produce the largest net radiative energy budget during the late transition and "wet" periods (October-February). The actual maximum occurred in December which is typically when the onset of the monsoon wet season occurs.

## Active Remote Sensing Instruments at Darwin

The suite of instruments at Darwin includes a millimeter cloud radar (MMCR) and a micropulse lidar (MPL). These instruments have not been operating continuously since installation but they were both operating during the transition into the summer monsoon and the early part of the wet season in support

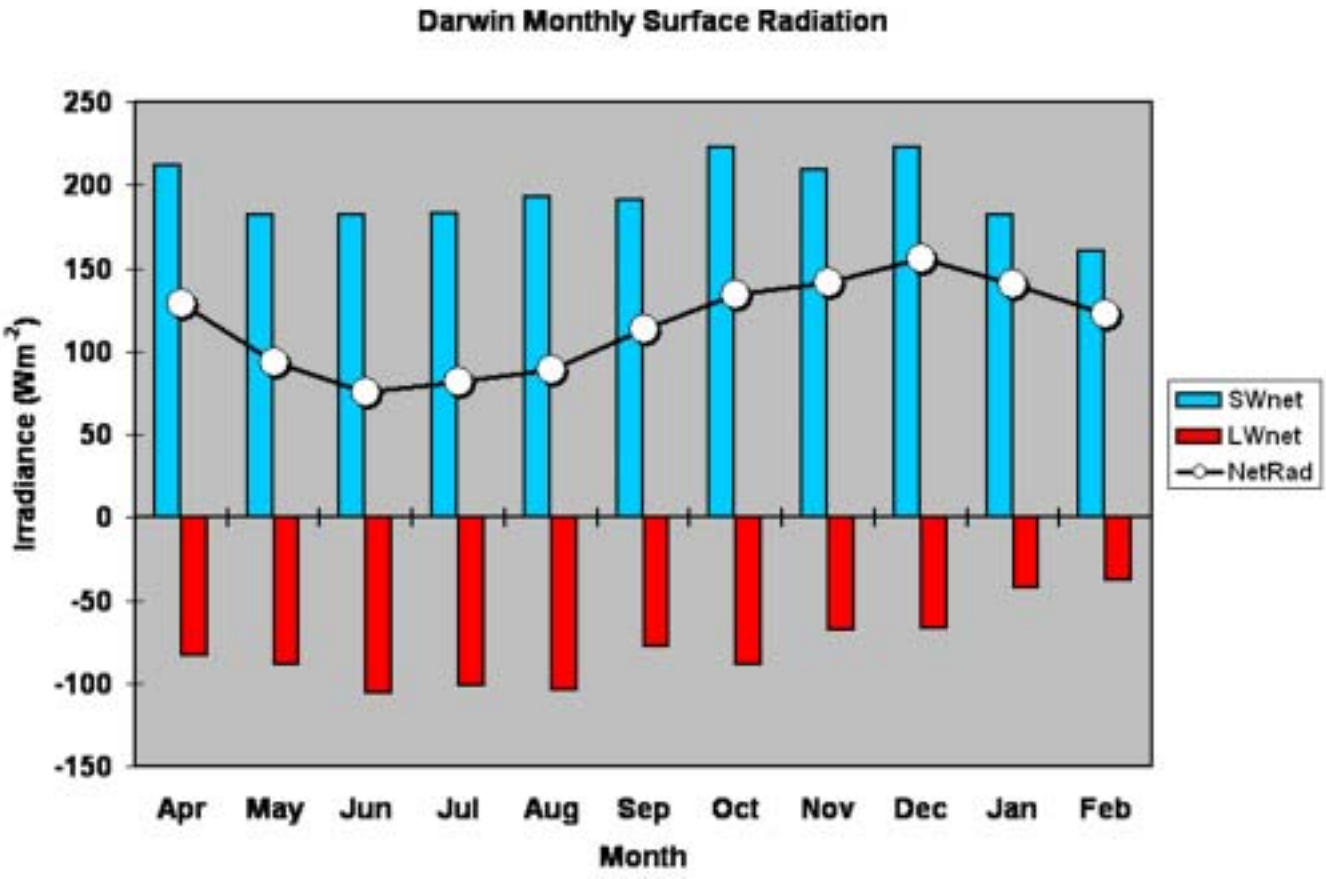


**Figure 10**. Net surface radiation fluxes for the SW (blue), LW (red), and their sum (circles). Net fluxes are defined as the downwelling flux minus the upwelling flux so positive values indicate a net absorption of energy by the surface while negative values indicate a net loss. All values are monthly averages.

of the Australian BMRC (Bureau of Meteorology Research Centre) -University of Wales EMERALD-2 (Egrett Microphysics Experiment with RAdiation Lidar and Dynamics) aircraft experiment. EMERALD-2 was held between November 15 and December 2, 2002, to study convection during the monsoon buildup season. Plots of coincident radar and lidar observations of a cirrus layer generated during the monsoon build-up season are shown in Figure 11. In this example, the cirrus observed is associated with the convective system, "Hector." Hector is a frequent deep convection feature tied to the Tiwi islands, approximately 75 km north of Darwin.

Similar to the Southern Great Plains site, Darwin offers a variety of meteorological observations which can augment the observations provided by the ARM instruments. Among the available resources in Darwin is a 5 cm, CPOL precipitation radar. Figure 12 shows a plot of 12 km altitude reflectivity from the Darwin CPOL radar for 0650 Universal Time Coordinates (UTC) on December 9. The Tiwi Islands are located at the northern end of the precipitation region depicted in this image.

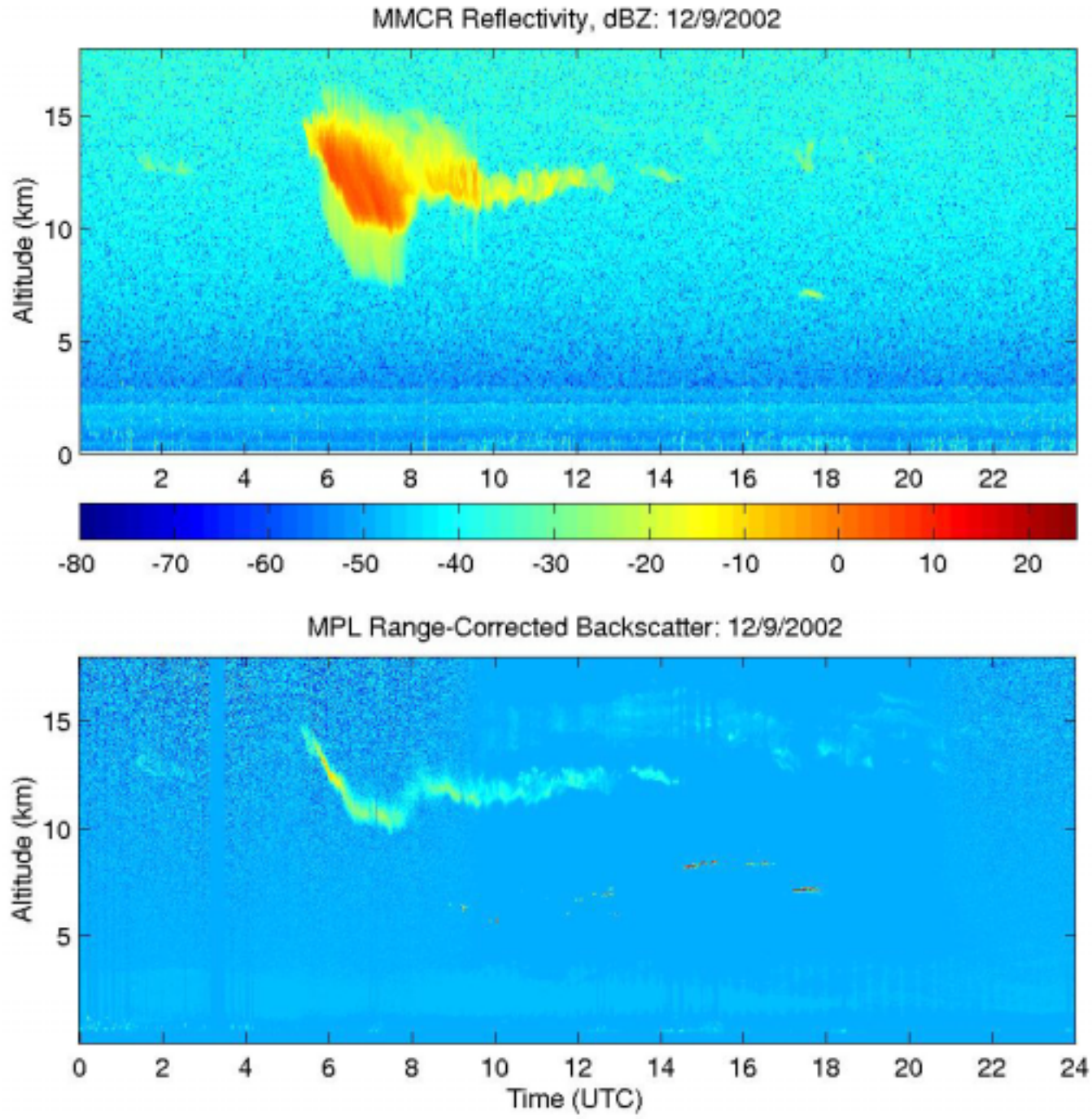


**Figure 11**. Observations from the millimeter cloud radar (top panel) and micropulse lidar (bottom panel) from December 9, 2002. In each figure, yellows and reds indicate the presence of clouds.

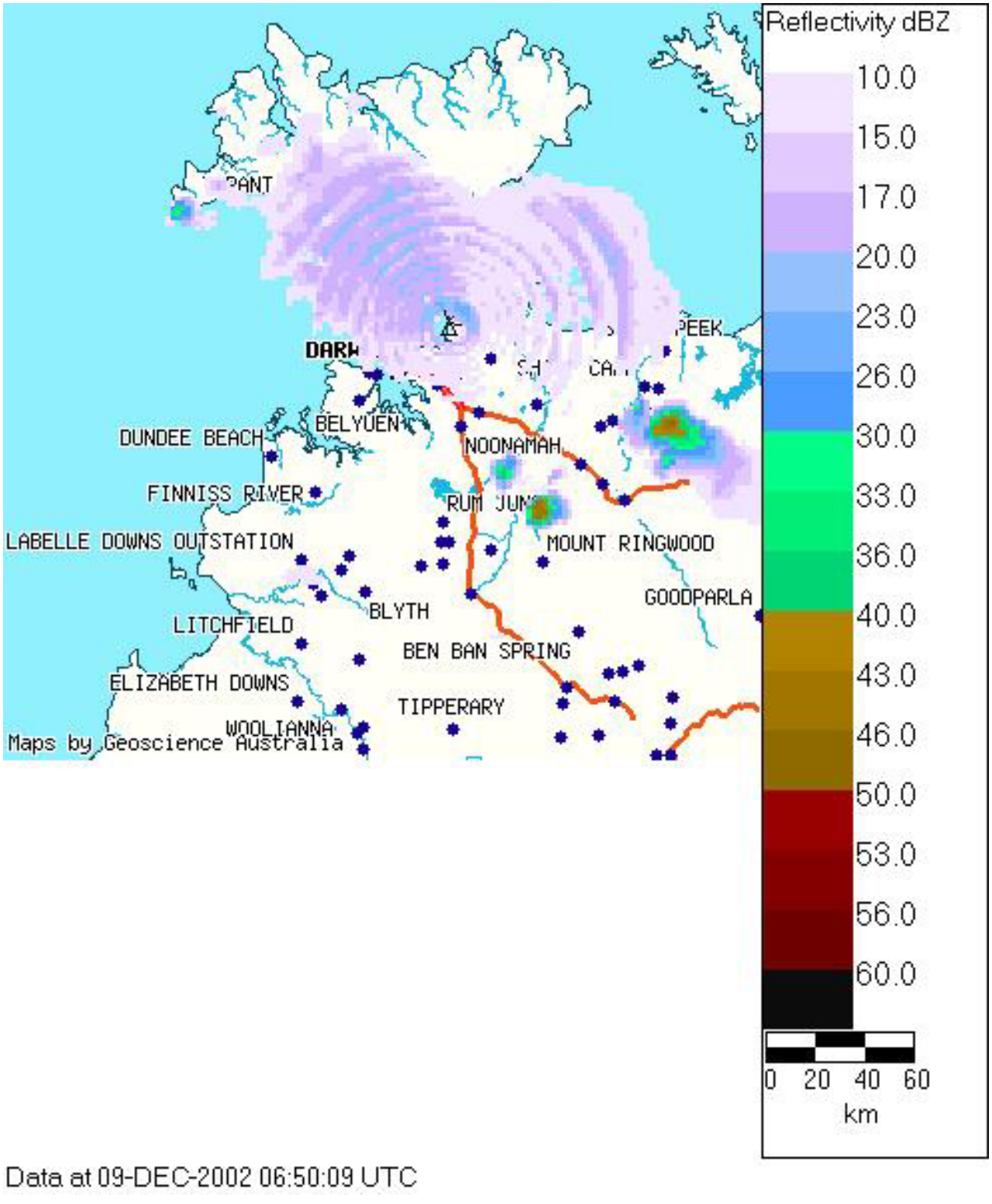


**Figure 12**. 12 km reflectivity from Darwin CPOL radar from 0650 UTC on December 9, 2002. (Image provided by Peter May of Australian Bureau of Meteorology).

## Conclusions

The data presented here illustrate the nature of the annual cycle at Darwin. The climatic characteristics of this site are very different than those found at Manus and Nauru which are both located closer to the equator and away from large land masses. Observations at Darwin will help understand the monsoon cycle and convection associated with the large islands of the Maritime Continent. As these phenomena are important for driving dynamics within the region, they impact convection at both Manus and Nauru. Darwin also provides a rich set of opportunities due to the auxiliary measurements in the region. In addition to the centimeter radar data discussed above, there are observations of aerosol and radiation. There is also a very long record of meteorological data. All of these factors will make Darwin a very interesting addition to the set of TWP sites.

## Corresponding Author

Jim Mather, Jim.Mather@pnl.gov, (509) 375-4533